ARTICLE

Differential Light-Induced Responses in Sectorial Inherited Retinal Degeneration

Eva Ramon[1], Arnau Cordomí[2], Mònica Aguilà[3], Sundaramoorthy Srinivasan[1], Xiaoyun Dong[1], Anthony T Moore[3,4], Andrew R Webster[3,4], Michael E Cheetham[3] and Pere Garriga[1]*

[1]Centre de Biotecnologia Molecular, Departament d'Enginyeria Química, Universitat Politècnica de Catalunya, Rambla de Sant Nebridi 22, 08222 Terrassa, Spain
[2]Laboratori de Medicina Computacional, Unitat de Bioestadística, Facultat de Medicina, Universitat Autònoma de Barcelona, 08193 Cerdanyola del Vallès, Spain
[3]UCL Institute of Ophthalmology, 11-43 Bath Street, London EC1V 9EL, UK
[4]Moorfields Eye Hospital, London UK

Address correspondence: Pere Garriga, Centre de Biotecnologia Molecular, Departament d'Enginyeria Química, Universitat Politècnica de Catalunya, Rambla de Sant Nebridi 22, 08222 Terrassa, Spain. Tel: +34 937398568; FAX: +34 937398225; E-mail: pere.garriga@upc.edu

Running Title: Molecular mechanism of sector retinitis pigmentosa

Keywords: G protein, GPCR (G-protein-coupled receptor), light exposure, membrane protein, protein stability, retinal degeneration, rhodopsin, signal transduction, visual pigments

Background: Two new rhodopsin mutations associated with the rare form sector retinitis pigmentosa (RP) have been found.
Results: Characterization of both rhodopsin mutant proteins shows different progression correlating with a different behavior of rhodopsin upon light exposure.
Conclusions: Light plays an important role in triggering sector RP.
Significance: Other mechanisms, in addition to protein misfolding, underlie GPCR dysfunction in pathological processes.

Retinitis pigmentosa (RP) is a group of genetically and clinically heterogeneous inherited degenerative retinopathies caused by abnormalities of photoreceptors or retinal pigment epithelium in the retina leading to progressive sight loss. Rhodopsin is the prototypical G-protein-coupled receptor located in the vertebrate retina and responsible for dim light vision. Here, novel M39R and N55K variants were identified as causing an intriguing sector phenotype of RP in affected patients, with selective degeneration in the inferior retina. In order to gain insights into the molecular aspects associated with this sector RP phenotype, whose molecular mechanism remains elusive, the mutations were constructed by site-directed mutagenesis, expressed in heterologous systems and studied by biochemical, spectroscopic and functional assays. M39R and N55K opsins had variable degrees of chromophore regeneration when compared to WT opsin, but showed no gross structural misfolding or altered trafficking. M39R showed a faster rate for transducin activation than WT rhodopsin with a faster metarhodopsinII decay, whereas N55K presented a reduced activation rate and an altered photobleaching pattern. N55K also showed an altered retinal release from the opsin binding pocket upon light exposure, affecting its optimal functional response. Our data suggest that these sector RP mutations cause different protein phenotypes which may be related to their different clinical progression. Overall, these findings illuminate the molecular mechanisms of sector RP associated with rhodopsin mutations.

RP refers to a group of inherited visual diseases that cause retinal degeneration and its incidence is around one of 4000 people (1). In the initial phase of the condition, RP patients have impaired dark adaptation and suffer from night blindness. Progression of the disease involves appearance of so-called tunnel vision, lack of outer lateral vision, the half-peripheral visual field is reduced to 30º-50°, and it can be accompanied by a decrease of the visual acuity. At later stages, signs include attenuated retinal vessels, and intraretinal bone pigment distributed circumferentially around the mid periphery in the fundus; myopia and astigmatism are also common (2).

Rhodopsin (Rh) is the prototypical member of the G-protein coupled receptor (GPCR) superfamily of membrane proteins, which includes over 900 members (3). The structures of several members of this superfamily have been resolved in the past decade using X-ray crystallography (4,5). Rh has been crystallized in various states, such as the dark-state form, the ligand-free form opsin structure, and the G protein-interacting conformation of opsin (6-8).

Rh is the light sensitive protein of the rod cell in the retina and is concentrated in the discs of the rod outer segment (9,10). In its basal resting state it consists of a polypeptide chain, opsin, and its cognate chromophore, the vitamin A aldehyde derivative 11-*cis*-retinal, which acts as an inverse agonist preventing G-protein activation in the dark (3,11). The retinal chromophore is responsible for light absorption in the visual process (12) and, upon photon capture, it isomerizes to its all-*trans* configuration yielding the active Rh photointermediate metarhodopsin II (MetaII) capable of binding and activating the G protein transducin (Gt) (13-15).

Mutations in the opsin gene are the most common cause of dominant RP. The large number of mutations and their different location along the polypeptide chain indicate a highly sophisticated arrangement of physicochemical interactions in the three dimensional structure of the native molecule. Although protein misfolding or altered trafficking are considered to be the major biochemical features of many RP mutations in Rh (16-19), some mutations do not induce major structural defects (20,21), but cause changes in G protein binding and activation (22,23), or the formation of altered photointermediates (24,25), among other phenotypes (17,25-28). Sector RP is an atypical form of RP, ranging from stationary to slowly progressive evolution of the retinal degenerative pattern, characterized by regional areas of bone spicule pigmentation, subnormal electroretinogram and visual-field defects, usually in the inferior quadrant of the retina (29,30).

It is important to obtain detailed knowledge of the characteristics of mutant proteins and to correlate the molecular defect observed with the clinical phenotype of the affected RP patients. For this purpose, we expressed, purified and characterized recombinant receptors containing mutations at amino acid N55 and M39, initially associated with sector RP, in order to determine the effect of these mutations on Rh stability and functionality. Residue $N55^{1.50}$ is part of the conserved GX_3N motif (31,32) in the first transmembrane helix (TM) of the receptor and has been proposed to be involved in a net of conserved allosteric interactions important for signal transduction (33). $M39^{1.34}$ is also located at the first TM, in one of the sites of the proposed retinal channel, where retinal can enter the protein and leave upon Schiff base (SB) breakage after photoactivation (34). We found that these two mutants show similar structural instability in the dark and significantly different photobleaching and G-protein activation responses. In particular, N55K shows a clear altered response to illumination in contrast to M39R behaviour. These differences at the molecular level may be correlated with the observed different clinical progressions for the two mutations.

Experimental procedures

Patients and clinical data- Patients and families were recruited from the inherited retinal clinics at Moorfields Eye Hospital as part of a larger study. Informed consent was obtained from all participants and all investigations were conducted in accordance with the principles of the Declaration of Helsinki. Institutional Review Board (IRB)/Ethics Committee approval was obtained from the Moorfields Eye Hospital Local Ethics Committee.

Patients and families with specific mutations in the *RHO* gene (RP4) were included in this study. Ophthalmological examination included best corrected visual acuity testing using Snellen charts, dilated fundus examination, color fundus photography (TRC-50IA; Topcon, Tokyo, Japan), spectral domain Optical Coherence Tomography (OCT) and fundus autofluorescence imaging (FAF). The Spectralis HRA+OCT with viewing module version 5.1.2.0 (Heidelberg Engineering, Heidelberg, Germany) was used to acquire tomographs. FAF images were acquired using the HRA2 and Spectralis HRA+OCT (encompasing a 30° × 30° and/or a 55° × 55° field; Heidelberg Engineering).

Materials- All chemicals were purchased from either Fisher Scientific (Madrid, Spain) or Sigma-Aldrich (St. Louis, MO, USA) except where stated. 11-*cis*-Retinal was kindly provided by Dr. R. Crouch and the National Eye Institute, National Institute of Health (USA). Purified Rh-1D4 was obtained from Cell Essentials (Boston, MA USA) and was coupled to CNBr-activated Sepharose 4B Fast Flow (Amersham Biosciences), secondary HRP conjugated goat antibody was provided by Santa Cruz Biotechnology (Heidelberg, Germany). *n*-Dodecyl-D-maltoside (DM) was purchased from Affimetrix (Maumee, OH, USA). The nanomer peptide corresponding to the last 9 amino acids of Rh was synthesized by Serveis Cientificotècnics (Universitat de Barcelona, Barcelona, Spain). Site-directed mutagenesis was performed by using Agilent Pfu polymerase and DpnI restriction enzyme and following QuickChange mutagenesis instructions (Agilent, Santa Clara, CA, USA). EndoH (cat numb. P0702L) and PNGaseF (P0704L) were from NEB (Hitchen, UK).

Cell culture materials- COS-1 cells were purchased from the American Type Culture Collection (Manassas, VA, USA), and SK-N-SH human Caucasian neuroblastoma cells from the European Collection of Cell Cultures (ECACC, Salisbury, UK). Tissue culture medium were provided from PAA (Austria) or Sigma Aldrich, antibiotics and Serum from Sigma-Aldrich (St. Louis, MO, USA), OPTIMEM Reduced Serum Media from Life Technologies (Madrid, Spain) and the polymer used for transfection, polyethylenimine 25 kDa (PEI), from Polysciences (Warrington, PA, USA). For cellular localization, the primary antibodies Rh-1D4 and Rh-4D2 against rod opsin were a gift from Robert Molday (Department of Biochemistry and Molecular Biology, University of British Columbia, Vancouver, Canada). Rabbit ploYclonal anti-BiP Anti-GRP78/BiP (GL-19) (cat. number G8918) was from Sigma. Goat anti-mouse Alexa Fluor 488 and goat anti-rabbit Alexa Fluor 594 secondary antibodies conjugated IgGs, Lipofectamine and Plus reagent were purchased from Invitrogen (Paisley, United Kingdom). Goat anti-mouse secondary antibody conjugated with horseradish peroxidase was from Pierce.

Buffers- Solutions used are defined as follows: Buffer A (137 mM NaCl, 2.7 mM KCl, 1.5 mM KH_2PO_4, and 8 mM Na_2HPO_4, pH 7.5), Buffer C (0.05% DM in buffer A, pH 7.5), and Buffer Gt (25 mM Tris pH 7.5, 100 mM NaCl, 5 mM magnesium acetate, 2.5 mM DTT, and 5μM [S^{35}]GTPγS (1.78 Ci/mmol)).

Construction, expression, and purification of mutant Rh- Opsin mutants were constructed with a site-directed mutagenesis kit (QuikChange, Stratagene) using a synthetic bovine opsin gene as a template (36). The expression and purification of the visual receptors were performed as previously described (37). Briefly, plasmids encoding the WT or mutant Rh genes were transfected into five COS-1 cells plates at 85% confluence, by using PEI with 30 μg of plasmid DNA per 145-cm plate. Cells were harvested 48–60 h after transfection, and pigments were reconstituted with 10 μM 11-*cis*-retinal in intact cells and then solubilized with 1% (w/v) DM in Buffer A. After centrifugation, the supernatant was incubated with a Sepharose 4B coupled to the Rh-1D4 antibody. The resin was washed with buffer C and pigments were subsequently eluted with the same buffer but containing 100 μM nonamer peptide.

Subcellular localization- SK-N-SH cells were maintained and transfected as described (35). 24 h after transfection, cells were fixed with 4% paraformaldehyde for 15 min and permeabilized in 0.5% Triton X-100 for 10 min. Nonspecific binding was blocked using blocking buffer (3% BSA and 10% serum of the secondary antibodies species in PBS) for 1 h. Rh-1D4 primary antibody (1:5000), anti-BiP (1:100) or Rh-4D2 primary antibody (1:100) in blocking buffer was added for 1 h. Secondary Alexa Fluor 488 or 594 were used at 1:1000 in blocking buffer for 1 h. Images were taken using a Carl Zeiss LSM 710 laser-scanning confocal microscope. The images were exported from LSM Browser and prepared using Adobe Photoshop and Illustrator CS4. Cell morphology studies scored the predominant localization of rod opsin on the plasma membrane (PM), or strong overlap with an endoplasmic reticulum (ER) marker, as a percentage of total transfected cells. Four fields of approximately 100 cells were counted for each condition.

Western blotting and glycosidase digestion- SK-N-SH transfected cells were lysed for 15 min at 4°C in PBS buffer containing 1% DM and 2% protease inhibitor cocktail in PBS. Cell lysates were centrifuged for 15 min at 12,000 x g and at 4ºC. For deglycosylation reactions, 10 µg total protein in DM soluble cell lysate was digested with EndoH or PNGase F for 2 h at 37°C. 10 µg total protein was added to 2x Laemmli loading buffer before being subjected to SDS-PAGE and Western blotting. For opsin immunodetection, Rh- 1D4 was used at 1:1500 and goat anti-mouse HRP (Pierce) was used at 1:50000 in 5% (w/v) Marvel Milk in PBS with 0.1 % (v/v) Tween buffer (PBS-T).

Absorbance and fluorescence spectroscopy instrumentation- All measurements were made on a Cary 100Bio spectrophotometer (Varian, Australia), equipped with water-jacketed cuvette holders connected to a circulating water bath. Temperature was controlled by a Peltier accessory connected to the spectrophotometer. All spectra were recorded in the 250nm–650 nm range with a bandwidth of 2 mm, a response time of 0.1 s, and a scan speed of 300 nm/min. The spectral ratio, which was used as a measure of pigment yield and stability, is defined as Absorbance at λ280nm divided by Absorbance at the visible λmax value. All fluorescence assays were performed by using a Photon Technologies QM-1 steady-state fluorescence spectrophotometer (PTI Technologies, Birmingham, NJ, USA). Sample temperature was controlled with a cuvette holder Peltier accessory TLC 50 (Quantum Northwest, Liberty Lake, WA, USA) connected to a hybrid liquid coolant system Reserator XT (Zalman, Garden Grove, CA, USA). All fluorescence spectra were carried out by exciting the samples for 2 s at λ295 nm and a bandwidth slit of 0.5 nm and blocking the excitation beam for 28 s with a beam shutter to avoid photobleaching of the sample (38). Tryptophan emission was monitored at λ330 nm and a bandwidth slit of 10 nm.

Spectral characterization of purified Rh-

Samples were bleached with a 150-watt power source equipped with an optic fiber guide and using a 495-nm cut-off filter. Dark-adapted pigments were illuminated for 30 s to ensure complete photoconversion to 380-nm absorbing species. Acidification was carried out, immediately after photobleaching, by the addition of H_2SO_4 2N.

Thermal bleaching assay- Rh thermal stability was monitored as previously described (39). Briefly, Rh bleaching rates, in the dark, were obtained by monitoring the decrease of absorbance at λmax of the visible spectral band as a function of time at 48 °C. Spectra were recorded every 2.5 min and half-life times were determined by fitting the experimental data to single-exponential curves using Sigma Plot version 11.0 (Systat Software, Chicago, IL, USA).

Hydroxylamine assay- A solution of hydroxylamine hydrochloride 1M, adjusted to pH 7, was added to dark-adapted samples in Buffer C (final concentration of 50 mM), and successive spectra were recorded every 2.5 min to monitor the loss of pigment (Amax) and formation of retinal oxime (A365 nm). Reactions were carried out in the dark at 20°C (37). Initial velocity was determined by fitting the experimental data to either a single-exponential curves or a linear plot using Sigma Plot version 11.0 (Systat Software).

MetaII decay measurements- The MetaII active conformation decay process was followed in real time by fluorescence spectroscopy (38). Briefly, 0.5 µM Rh in Buffer C was kept at 20°C for 10 min and illuminated for 30 s. The $t_{1/2}$ values of Trp fluorescence increase, due to retinal release, were determined by fitting the experimental data to a single-exponential curve using Sigma Plot version 11.0 (Systat Software, Inc., Chicago, IL, USA).

Gt activation assay- G protein activation was determined in COS-1 cell membranes, prepared as previously described (37) and the ability of opsin and Rh to activate Gt was monitored with a radionucleotide filter binding assay by measuring the uptake of [S^{35}]GTPγS by Gt purified from bovine retinas. The assays were performed by mixing 10 nM Rh or opsin in membranes with 500 nM Gt in Gt buffer at room temperature. Reactions were initiated by the addition of Rh or opsin in the dark, and samples were filtrated after different incubation times, either in the dark or after illumination, to determine the amount of bound [S^{35}]GTPγS.

Results

Clinical Findings- Of 73 unrelated families presenting to the inherited retinal disease clinics at Moorfields with retinal degeneration, in which *RHO* was the established causative gene, three families were found to harbour the variant p.N55K. Clinical data were available on five affected individuals from these three families. In family GC18466, the female proband first noticed nyctalopia in the 30s and was diagnosed with RP at age 35. Visual acuities were normal when measured at age 45 years. A *de novo* mutation was assumed because neither parent had symptoms, nor did they harbour the mutation. The fundus and OCT findings for this patient are shown in Fig. 1A-D, G-H, and I-J. Two from three children were found presymptomatically to have inferior retinal pigmentation suggestive of RP at ages 13 and 14 years. In family GC16563, the 26 year old female proband was examined by an optometrist following the incidental finding of retinal signs in her mother. Despite inferior retinal pigmentation, no symptoms had developed up until the last review at age 39 years (Fig. 1E-F). Electroretinography ISCEV standard at this age was

normal. In the third family, GC17079, a female patient at the age of 37 years had night-blindness and field loss, the latter enough to fail the UK driving standard. Visual acuities were 6/9 right, 6/5 left. There was a family history compatible with autosomal dominant segregation but no other relatives were examined.

Of the 73 unrelated *RHO* families, 6 families were identified with p.M39R heterozygous mutations (GC97, 109, 414, 1379, 4740 and 19172). All of them consistently showed an inferior hemisphere that was more affected than the superior. The eye fundus autofluorescence images for patients from some of these families are shown in Fig. 2. In contrast to p.N55K, however, the retinal degeneration was more severe and progressed to the superior retina with age (Fig 2).

Molecular modelling of the RP mutants-

The repertoire of Rh crystal structures (7,8,40-43) suggest the existence of a channel between TMs 1 and 7 that retinal uses to entry/exit its binding cavity (34). M39 lies at the mouth of this channel, where the crystal structures revealed the presence of fatty acids, lipids and detergent molecules (Fig. 3A), supporting the hypothesis that this region might accommodate hydrophobic retinal in an intermediate step. Fig. 3B shows that F293, adjacent to M39, exhibits a conformational change upon receptor activation. Specifically, in the crystal structures representing the inactive states (Fig. 3B, orange cartoon), F293 is buried within the binding pocket and closes the channel by interacting with L40, whereas in those representing active structures (Fig. 3B, red cartoon), F293 has moved towards the membrane exposed face of TM1 and interacts with Y43 (Fig. 3B). This conformational change is accompanied by a parallel shift of TMs 6 and 7 towards TM1. Consequently, the presence of a positively charged residue, such as R39, nearby this network, would potentially alter the exit/entry of retinal through the ligand channel, and it may also affect the conformational changes involving helical motions ensuing receptor photoactivation.

Three highly conserved residues, throughout the GPCRs superfamily, at the cytoplasmic side of the receptor, $N55^{1.50}$ (98%), $D83^{2.50}$ (92%) and $N302^{7.49}$ (77%) define a region with intimate contact between TMs 1, 2 and 7, which involve also various highly conserved water molecules (44) (Fig. 3C). In the N55K substitution, the Lys side-chain would interfere with these contacts and form a salt bridge with $D83^{2.50}$.

On the other hand, our molecular models suggest that the M39R substitution may alter the TM1-TM7 interface and the network of interactions between TMs 1, 6 and 7, suggesting problems on receptor stability, and the rate of both Gt activation and retinal release, due to the location of M39R in the proposed entry/exit retinal channel (34).

Subcellular localization of RP mutants in SK-N-SH cells- The heterologous expression of rod opsin in cell culture can be used to monitor protein biogenesis, traffic and facilitate protein purification for functional studies. We used SK-N-SH neuroblastoma cells to study the biogenesis, degradation, aggregation and traffic of WT and mutant forms, as this cell line has been used extensively in the past (e.g. (37)). WT rod opsin was mainly localized on the PM (94% of transfected cells) and did not overlap with the ER marker BiP (Fig. 4A and C). Occasionally WT rod

opsin was predominantly retained in the ER (5% of cells) or formed intracellular inclusions (3% of cells) (Fig. 4A and C). The M39R and N55K amino acid substitutions in rod opsin did not have a major effect on traffic in SK-N-SH cells (Fig. 4A). Both mutants were localized to the PM in the majority of cells (88% and 80% respectively) and only a few cells showed predominant retention in the ER and overlap with BiP staining or inclusion formation (Fig. 4A and C). The traffic of WT, N55K and M39R rod opsin to the PM was confirmed by staining non-permeabilized transfected SK-N-SH cells with the Rh antibody 4D2, which recognizes an extracellular epitope (Fig. 4B). The electrophoretic mobility of the mutant proteins on Western blotting was similar to WT rod opsin (Fig. 4D); but the expression level was generally reduced. Digestion of cell lysates with the glycosidase EndoH showed that, like WT, most of the N55K and M39R rod opsin protein was EndoH resistant and therefore had trafficked beyond the ER (Fig. 4D).

UV-vis spectral characterization of purified mutants- The RP mutant opsins were purified and their UV-visible spectra investigated (Fig. 5). N55K and M39R were purified at a lower yield when compared to WT, and they also had a ratio A280/Amax of 5.4 and 6, approximately 2.2 and 2.4-fold higher when compared to the WT ratio, respectively (Table 1). This could indicate folding problems in these mutants that may not allow complete regeneration with 11-*cis*-retinal. The dark spectra of N55K showed a blue shift of 3 nm in the visible absorbance band when compared to that of the WT. Upon illumination, the N55K spectrum also showed a specific behavior, without a complete conversion of the visible band to the 380-nm absorbing species. This remaining band, observed upon illumination, had a similar visible wavelength maximum as the dark pigment, blue-shifted only 3 nm, suggesting conversion to a photointermediate with a retinal binding pocket similar to the dark pigment, including the presence of a protonated SB linkage. This behavior is different from other RP mutants, such as G51V and G89D, that also showed a blue-shifted photointermediate, possibly reflecting changes in the retinal binding pocket (24,45). The M39R mutant had photobleaching behavior similar to that of the WT protein (compare insets in Fig. 5).

Thermal and chemical stability in the dark- The chemical reagent hydroxylamine, added in the dark, decreased the visible maximal absorbance, especially in the case of N55K. Here, the initial rate of the hydroxylamine-induced bleaching process was about 50-fold faster than that of WT Rh (Table 1 and Fig. 6A), suggesting that the SB in this mutant is more exposed to the environment so the reagent can enter, break the SB and sequester the retinal from the binding pocket. Hydroxylamine also affected the chemical stability of M39R mutant but to a lesser extent than N55K. Thermal bleaching was studied at 48ºC, by monitoring the decrease of absorbance at the visible λmax over time. Both RP mutants were unstable in the dark-state (Table 1 and Fig. 6B). In order to improve protein stability, 1,2-didocosahexaenoylsn-glycero-3-phosphocholine (DDHA-PC) lipid was used, previously shown to increase Rh stability (46), but it did not help to stabilize N55K, when compared to Rh from rod outer segments (data not shown).

MetaII stability- The stability of the active state of purified Rh was measured by monitoring the fluorescence increase upon illumination (Fig. 7). MetaII stability $t_{1/2}$ of N55K mutant was similar to

that of WT Rh, showing that this mutation does not affect initial retinal release upon illumination, whereas for the M39R mutant the release occurred faster ($t_{1/2}$= 10.8 min). When a fluorescence plateau was reached, hydroxylamine was added to test whether there was still retinal remaining in the binding pocket. Strikingly, N55K reached a plateau at lower fluorescence intensity and showed an additional increase in Trp fluorescence emission, upon hydroxylamine addition to the sample, reflecting the presence of residual retinal in the binding pocket for a long time after bleaching (Fig. 7C). In order to determine if this could be a differential feature of sector RP mutants, retinal release was compared to that of the G51V RP mutant, position G51 is located one helical turn below N55 and G51V also showed a different photobleaching behavior when compared to WT similar to N55K (45). In this case, however, the G51V MetaII assay showed a similar behavior to WT (data not shown).

Gt activation for WT and mutants- Gt activation by Rh and opsin forms was monitored by using a GTPγS^{35} binding assay where the protein was incubated in a mixture containing the G-protein. The amount of GTPγS^{35} bound was determined by a radioactive binding assay (37). The opsin form (i.e. with no retinal) was used in order to determine whether the mutations caused constitutive activity. We observed that these mutations do not activate Gt in the absence of the ligand and thus they are not constitutively active (Fig. 8). Photoactivated mutant Rh activated Gt but with altered kinetics. Compared to the WT, M39R activated Gt at a faster rate, whereas N55K activated the G protein at a slower rate, 3.4 and 0.3-fold respectively (Table 1). The N55K result is compatible with the proposed importance of the conserved N$^{1.50}$ position in G-protein activation (47-49).

Discussion

Understanding the molecular mechanism(s) underlying retinal degeneration is the first step towards finding an efficient treatment for RP. Here, we analyzed the consequences on the stability and functionality of Rh caused by the two newly identified RP mutations, M39R and N55K, located in the first TM of the receptor. Spectral characterization showed that M39R and N55K behave differently than the WT showing decreased chromophoric visible bands than the WT protein after purification in detergent solution. In spite of the fact that the pattern observed in our spectra could be compatible with some sort of protein misfolding, as previously reported for other RP mutations, such as T58R (50), the results obtained from the cellular localization clearly indicate that these mutants trafficked to the PM at a similar level to WT opsin, suggesting that these mutations do not significantly alter the folding of Rh in the ER of cell culture systems. Moreover, Western blot analysis of these mutant proteins showed a slightly different mobility and lower level of expression when compared to the WT, which may reflect differences in the degradation rate and/or glycosylation pattern (Fig. 4C). However, digestion with the glycosidase EndoH, which digests ER resident glycoproteins, confirmed that most of the N55K and M39R mutant protein trafficked normally. Therefore, if the lower expression levels are due to enhanced degradation this must be

efficient, as the mutant proteins did not accumulate in the ER. Taking all this evidence into account, we suggest that the decrease in the level of chromophore present in the purified samples is potentially due to protein instability during the purification process, rather than an ER folding problem. Because chromophore stability of these two mutants was 90% lower than that of WT when treated at 48ºC (Table 1), but they still reached the PM in over 80% of cells (in contrast with the ER retention levels seen as one of the key features for class II mutants (28)), both mutants are more consistent with a class IV phenotype of near normal native folding but with inherent structural instability (20). The crystal structures suggest that the effects of M39R on Rh could be related to the involvement of the residue in a proposed entry/exit channel for retinal between TMs 1 and 7 (34).

In the case of the N55K substitution, the mutation at the conserved $N^{1.50}$ residue affected retinal release during the MetaII decay. Addition of hydroxylamine to the sample, after the fluorescence signal had reached a plateau, caused further release of retinal, indicating that some retinal was still present inside the protein a long time after photobleaching. This retinal trapping would undoubtedly alter the visual cycle, affecting the normal retinal turnover rate (51). This behavior was not detected for the G51V RP mutant (45) located only one helix turn away from N55, which also shows a different photobleaching behavior when compared to WT Rh. In this case, the similar retinal release pattern to WT suggests that the retinal trapping found in the N55K mutant may be a distinctive feature of this form of sector RP. Our molecular modelling results suggest that the Lys residue interferes in the network between TMs 1, 2 and 7, due to the proximity of N55, D83, and N302, including water molecules (44). Additionally, Fourier-transform infrared difference spectra experiments indicated that $D83^{2.50}$ should be protonated (52), which would be affected by the introduction of Lys in this environment.

The molecular differences observed for the N55K and M39R mutated proteins can be associated with the physico-chemical nature of the introduced amino acid residue as a result of the mutation. Both mutations are located at the same helix (TM1) of Rh, and both introduce positively charged amino acids of a similar volume. However, the N55K substitution appears to have a specific behavior. Interestingly, another mutation to Lys in the TM domain of Rh, M207K, was shown to have an unusual autosomal dominant retinal phenotype characterized by a heterogeneous distribution (53). It is possible that mutations introducing a Lys, at the transmembrane core of Rh, cause unusual phenotypes as a result of affecting the entry/exit paths of the retinal chromophore after isomerization and SB hydrolysis.

The intrinsic structural features of the receptor-bound chromophore, in some Rh RP mutants, could result in differences in keeping the retinal in its binding pocket and altering its release mechanism. And this could be the starting cause of the retinal degeneration process. Thus, the presence of unstable free opsin proteins, either in the dark or at different stages of the photoactivation process, could result in protein aggregation and ultimately in cell death. The presence of fully functional Rh is important for maintaining healthy photoreceptor cells. Rh knock-

out mice have been reported to be unable to generate photoreceptor rod outer segments (54). In the case of N55K, a critical factor, in addition to its inherent instability, is the altered behavior upon illumination (and associated altered retinal release) that could affect the Rh photocycle disrupting normal retinal accessibility and protein turnover.

Besides the structural consequences of these mutations, the big question is why the affected region is restricted to a specific part of the retina when the Rh mutation is present all over the retina. There is a clear variability in the clinical phenotypes of the novel sector RP mutations studied. M39R, for instance, initially shows a sector phenotype but over time the degenerative process spreads to the whole retina and the patient develops a classical RP phenotype. On the other hand, P23H, the most common autosomal dominant RP mutation, has been described to be heterogeneous, some people showed a sector phenotype and other people typical RP form, suggesting the influence of external factors (55). To date, most of the studies have focused on the idea that light is an important external factor underlying sector RP (56,57), and a different light distribution has been proposed in the different sections of the retina, based on a theoretical model (58). Previous reports on mice carrying a transgene with the P23H mutation involved housing the animals under overhead light or in the dark and higher photoreceptor degeneration was observed in the inferior retina of mice reared under an overhead light (59). Moreover, a recent study in *X. Laevis* has provided further evidence of the effects of light on sector RP derived degeneration (60). In spite of these studies, no definitive answer has been provided about the link between light and sector RP, and it is not clear whether the direct action of light on Rh, or other unknown light-sensitive factors located in the retina, may cause this particular phenotype. The detailed molecular basis of light-dependent translocation of proteins from the inner segment to the outer segment in photoreceptor cells, such as arrestin (61), or from the outer segment to the inner segment, like Gt (62), is still largely undeciphered, but appears to be a fine-regulated machine and a small change in one of the partners could significantly affect the function of others. Here, we show that N55K presents a different behavior upon illumination by forming a photointermediate unable to completely finish the retinal release process from its binding pocket. We suggest that this supports the direct action of light on Rh as the trigger for the observed sector phenotype. Thus, different times and/or dose exposures to light, in combination with malfunction of the receptor due to the mutation, may be the cause of sector RP. The mechanism could also indirectly involve other light-sensitive proteins or factors so far unidentified, but confirming this aspect would require further investigation.

In view of the clinical phenotypes observed for the two mutations reported herein, we can ask the question, is sector RP really that uncommon? Our results emphasize that sector RP etiology is not crystal clear. It could be that in many instances sector RP is an initial step, before the development of a typical RP phenotype. Some mutations might cause unnoticeable effects early in disease, and RP would be diagnosed as a typical form later on after severe visual impairment arises (52). For example, in one M39R family, the fundus of a son shows a sector phenotype (Fig.

2A), whereas his father (Fig. 2E) has a more typical RP form. Time will tell if the son will develop the typical form like his father or will remain as sector RP. According to our findings, we believe that the son will develop typical RP when older. In contrast, N55K appears relatively stable and restricted to the inferior retina in the families we have studied and the protein has unique properties upon illumination, suggesting this is genuine sector RP.

REFERENCES

1. Petrs-Silva, H., and Linden, R. (2014) Advances in gene therapy technologies to treat retinitis pigmentosa. *Clin Ophthalmol* **8**, 127-136
2. Berson, E. L. (1993) Retinitis pigmentosa. The Friedenwald Lecture. *Investigative ophthalmology & visual science* **34**, 1659-1676
3. Palczewski, K. (2006) G protein-coupled receptor rhodopsin. *Annu Rev Biochem* **75**, 743-767
4. Katritch, V., Cherezov, V., and Stevens, R. C. (2013) Structure-function of the G protein-coupled receptor superfamily. *Annual review of pharmacology and toxicology* **53**, 531-556
5. Rosenbaum, D. M., Rasmussen, S. G., and Kobilka, B. K. (2009) The structure and function of G-protein-coupled receptors. *Nature* **459**, 356-363
6. Park, J. H., Scheerer, P., Hofmann, K. P., Choe, H. W., and Ernst, O. P. (2008) Crystal structure of the ligand-free G-protein-coupled receptor opsin. *Nature* **454**, 183-187
7. Scheerer, P., Park, J. H., Hildebrand, P. W., Kim, Y. J., Krauss, N., Choe, H. W., Hofmann, K. P., and Ernst, O. P. (2008) Crystal structure of opsin in its G-protein-interacting conformation. *Nature* **455**, 497-502
8. Choe, H. W., Kim, Y. J., Park, J. H., Morizumi, T., Pai, E. F., Krauss, N., Hofmann, K. P., Scheerer, P., and Ernst, O. P. (2011) Crystal structure of metarhodopsin II. *Nature* **471**, 651-655
9. Hargrave, P. A. (2001) Rhodopsin structure, function, and topography the Friedenwald lecture. *Investigative ophthalmology & visual science* **42**, 3-9
10. Sakmar, T. P., Menon, S. T., Marin, E. P., and Awad, E. S. (2002) Rhodopsin: insights from recent structural studies. *Annual review of biophysics and biomolecular structure* **31**, 443-484
11. Matsuyama, T., Yamashita, T., Imai, H., and Shichida, Y. (2010) Covalent bond between ligand and receptor required for efficient activation in rhodopsin. *The Journal of biological chemistry* **285**, 8114-8121
12. Wald, G. (1968) Molecular basis of visual excitation. *Science* **162**, 230-239

13. Jastrzebska, B., Tsybovsky, Y., and Palczewski, K. (2010) Complexes between photoactivated rhodopsin and transducin: progress and questions. *Biochem J* **428**, 1-10
14. Ahuja, S., and Smith, S. O. (2009) Multiple switches in G protein-coupled receptor activation. *Trends in pharmacological sciences* **30**, 494-502
15. Tesmer, J. J. (2010) The quest to understand heterotrimeric G protein signaling. *Nature structural & molecular biology* **17**, 650-652
16. Carrell, R. W. (2005) Cell toxicity and conformational disease. *Trends Cell Biol* **15**, 574-580
17. Krebs, M. P., Holden, D. C., Joshi, P., Clark, C. L., 3rd, Lee, A. H., and Kaushal, S. (2010) Molecular mechanisms of rhodopsin retinitis pigmentosa and the efficacy of pharmacological rescue. *J Mol Biol* **395**, 1063-1078
18. Surguchev, A., and Surguchov, A. (2010) Conformational diseases: looking into the eyes. *Brain Res Bull* **81**, 12-24
19. Gregersen, N., Bross, P., Vang, S., and Christensen, J. H. (2006) Protein misfolding and human disease. *Annu Rev Genomics Hum Genet* **7**, 103-124
20. Mendes, H. F., van der Spuy, J., Chapple, J. P., and Cheetham, M. E. (2005) Mechanisms of cell death in rhodopsin retinitis pigmentosa: implications for therapy. *Trends Mol Med* **11**, 177-185
21. Green, E. S., Menz, M. D., LaVail, M. M., and Flannery, J. G. (2000) Characterization of rhodopsin mis-sorting and constitutive activation in a transgenic rat model of retinitis pigmentosa. *Invest Ophthalmol Vis Sci* **41**, 1546-1553
22. Fain, G. L., and Lisman, J. E. (1999) Light, Ca2+, and photoreceptor death: new evidence for the equivalent-light hypothesis from arrestin knockout mice. *Investigative ophthalmology & visual science* **40**, 2770-2772
23. Lisman, J., and Fain, G. (1995) Support for the equivalent light hypothesis for RP. *Nature medicine* **1**, 1254-1255
24. Hwa, J., Garriga, P., Liu, X., and Khorana, H. G. (1997) Structure and function in rhodopsin: packing of the helices in the transmembrane domain and folding to a tertiary structure in the intradiscal domain are coupled. *Proc Natl Acad Sci U S A* **94**, 10571-10576
25. Travis, G. H. (1998) Mechanisms of cell death in the inherited retinal degenerations. *Am J Hum Genet* **62**, 503-508
26. Tai, A. W., Chuang, J. Z., Bode, C., Wolfrum, U., and Sung, C. H. (1999) Rhodopsin's carboxy-terminal cytoplasmic tail acts as a membrane receptor for

cytoplasmic dynein by binding to the dynein light chain Tctex-1. *Cell* **97**, 877-887

27. Bessant, D. A., Khaliq, S., Hameed, A., Anwar, K., Payne, A. M., Mehdi, S. Q., and Bhattacharya, S. S. (1999) Severe autosomal dominant retinitis pigmentosa caused by a novel rhodopsin mutation (Ter349Glu). Mutations in brief no. 208. Online. *Human mutation* **13**, 83
28. Sung, C. H., Davenport, C. M., and Nathans, J. (1993) Rhodopsin mutations responsible for autosomal dominant retinitis pigmentosa. Clustering of functional classes along the polypeptide chain. *The Journal of biological chemistry* **268**, 26645-26649
29. Van Woerkom, C., and Ferrucci, S. (2005) Sector retinitis pigmentosa. *Optometry* **76**, 309-317
30. Moore, A. T., Fitzke, F. W., Kemp, C. M., Arden, G. B., Keen, T. J., Inglehearn, C. F., Bhattacharya, S. S., and Bird, A. C. (1992) Abnormal dark adaptation kinetics in autosomal dominant sector retinitis pigmentosa due to rod opsin mutation. *The British journal of ophthalmology* **76**, 465-469
31. Ballesteros, J. A., and Weinstein, H. (1995) Integrated methods for the construction of three-dimensional models and computational probing of structure-function relations in G protein-coupled receptors. *Methods in Neuroscience* **25**, 366-428
32. Tikhonova, I. G., Best, R. B., Engel, S., Gershengorn, M. C., Hummer, G., and Costanzi, S. (2008) Atomistic insights into rhodopsin activation from a dynamic model. *Journal of the American Chemical Society* **130**, 10141-10149
33. Ciarkowski, J., Drabik, P., Gieldon, A., Kazmierkiewicz, R., and Slusarz, R. (2001) Signal transmission via G protein-coupled receptors in the light of rhodopsin structure determination. *Acta biochimica Polonica* **48**, 1203-1207
34. Hildebrand, P. W., Scheerer, P., Park, J. H., Choe, H. W., Piechnick, R., Ernst, O. P., Hofmann, K. P., and Heck, M. (2009) A ligand channel through the G protein coupled receptor opsin. *PLoS One* **4**, e4382
35. Mendes, H. F., and Cheetham, M. E. (2008) Pharmacological manipulation of gain-of-function and dominant-negative mechanisms in rhodopsin retinitis pigmentosa. *Human molecular genetics* **17**, 3043-3054
36. Oprian, D. D., Molday, R. S., Kaufman, R. J., and Khorana, H. G. (1987) Expression of a synthetic bovine rhodopsin gene in monkey kidney cells. *Proc Natl Acad Sci U S A* **84**, 8874-8878
37. Toledo, D., Ramon, E., Aguila, M., Cordomi, A., Perez, J. J., Mendes, H. F., Cheetham, M. E., and Garriga, P. (2011) Molecular mechanisms of disease for

mutations at Gly-90 in rhodopsin. *The Journal of biological chemistry* **286**, 39993-40001

38. Farrens, D. L., and Khorana, H. G. (1995) Structure and function in rhodopsin. Measurement of the rate of metarhodopsin II decay by fluorescence spectroscopy. *The Journal of biological chemistry* **270**, 5073-5076
39. Reyes-Alcaraz, A., Martinez-Archundia, M., Ramon, E., and Garriga, P. (2011) Salt effects on the conformational stability of the visual G-protein-coupled receptor rhodopsin. *Biophysical journal* **101**, 2798-2806
40. Li, J., Edwards, P. C., Burghammer, M., Villa, C., and Schertler, G. F. (2004) Structure of bovine rhodopsin in a trigonal crystal form. *J Mol Biol* **343**, 1409-1438
41. Okada, T., Sugihara, M., Bondar, A. N., Elstner, M., Entel, P., and Buss, V. (2004) The retinal conformation and its environment in rhodopsin in light of a new 2.2 A crystal structure. *J Mol Biol* **342**, 571-583
42. Okada, T., Fujiyoshi, Y., Silow, M., Navarro, J., Landau, E. M., and Shichida, Y. (2002) Functional role of internal water molecules in rhodopsin revealed by X-ray crystallography. *Proc Natl Acad Sci U S A* **99**, 5982-5987
43. Standfuss, J., Edwards, P. C., D'Antona, A., Fransen, M., Xie, G., Oprian, D. D., and Schertler, G. F. (2011) The structural basis of agonist-induced activation in constitutively active rhodopsin. *Nature* **471**, 656-660
44. Pardo, L., Deupi, X., Dolker, N., Lopez-Rodriguez, M. L., and Campillo, M. (2007) The role of internal water molecules in the structure and function of the rhodopsin family of G protein-coupled receptors. *Chembiochem : a European journal of chemical biology* **8**, 19-24
45. Bosch-Presegue, L., Ramon, E., Toledo, D., Cordomi, A., and Garriga, P. (2011) Alterations in the photoactivation pathway of rhodopsin mutants associated with retinitis pigmentosa. *The FEBS journal* **278**, 1493-1505
46. Sanchez-Martin, M. J., Ramon, E., Torrent-Burgues, J., and Garriga, P. (2013) Improved conformational stability of the visual G protein-coupled receptor rhodopsin by specific interaction with docosahexaenoic acid phospholipid. *Chembiochem : a European journal of chemical biology* **14**, 639-644
47. Nygaard, R., Frimurer, T. M., Holst, B., Rosenkilde, M. M., and Schwartz, T. W. (2009) Ligand binding and micro-switches in 7TM receptor structures. *Trends in pharmacological sciences* **30**, 249-259
48. Cabana, J., Holleran, B., Beaulieu, M. E., Leduc, R., Escher, E., Guillemette, G., and Lavigne, P. (2013) Critical hydrogen bond formation for activation of the

angiotensin II type 1 receptor. *The Journal of biological chemistry* **288**, 2593-2604

49. Rasmussen, S. G., Choi, H. J., Rosenbaum, D. M., Kobilka, T. S., Thian, F. S., Edwards, P. C., Burghammer, M., Ratnala, V. R., Sanishvili, R., Fischetti, R. F., Schertler, G. F., Weis, W. I., and Kobilka, B. K. (2007) Crystal structure of the human beta2 adrenergic G-protein-coupled receptor. *Nature* **450**, 383-387
50. Sung, C. H., Schneider, B. G., Agarwal, N., Papermaster, D. S., and Nathans, J. (1991) Functional heterogeneity of mutant rhodopsins responsible for autosomal dominant retinitis pigmentosa. *Proc Natl Acad Sci U S A* **88**, 8840-8844
51. Perusek, L., and Maeda, T. (2013) Vitamin A derivatives as treatment options for retinal degenerative diseases. *Nutrients* **5**, 2646-2666
52. Fahmy, K., Jager, F., Beck, M., Zvyaga, T. A., Sakmar, T. P., and Siebert, F. (1993) Protonation states of membrane-embedded carboxylic acid groups in rhodopsin and metarhodopsin II: a Fourier-transform infrared spectroscopy study of site-directed mutants. *Proc Natl Acad Sci U S A* **90**, 10206-10210
53. Audo, I., Friedrich, A., Mohand-Said, S., Lancelot, M. E., Antonio, A., Moskova-Doumanova, V., Poch, O., Bhattacharya, S., Sahel, J. A., and Zeitz, C. (2010) An unusual retinal phenotype associated with a novel mutation in RHO. *Archives of ophthalmology* **128**, 1036-1045
54. Humphries, M. M., Rancourt, D., Farrar, G. J., Kenna, P., Hazel, M., Bush, R. A., Sieving, P. A., Sheils, D. M., McNally, N., Creighton, P., Erven, A., Boros, A., Gulya, K., Capecchi, M. R., and Humphries, P. (1997) Retinopathy induced in mice by targeted disruption of the rhodopsin gene. *Nature genetics* **15**, 216-219
55. Vaughan, D. K., Coulibaly, S. F., Darrow, R. M., and Organisciak, D. T. (2003) A morphometric study of light-induced damage in transgenic rat models of retinitis pigmentosa. *Investigative ophthalmology & visual science* **44**, 848-855
56. Paskowitz, D. M., LaVail, M. M., and Duncan, J. L. (2006) Light and inherited retinal degeneration. *The British journal of ophthalmology* **90**, 1060-1066
57. Cideciyan, A. V., Jacobson, S. G., Aleman, T. S., Gu, D., Pearce-Kelling, S. E., Sumaroka, A., Acland, G. M., and Aguirre, G. D. (2005) In vivo dynamics of retinal injury and repair in the rhodopsin mutant dog model of human retinitis pigmentosa. *Proc Natl Acad Sci U S A* **102**, 5233-5238
58. Schwartz, L., Boelle, P. Y., D'Hermies, F., Ledanois, G., and Virmont, J. (2003) Blue light dose distribution and retinitis pigmentosa visual field defects: an hypothesis. *Medical hypotheses* **60**, 644-649

59. Naash, M. L., Peachey, N. S., Li, Z. Y., Gryczan, C. C., Goto, Y., Blanks, J., Milam, A. H., and Ripps, H. (1996) Light-induced acceleration of photoreceptor degeneration in transgenic mice expressing mutant rhodopsin. *Investigative ophthalmology & visual science* **37**, 775-782
60. Tam, B. M., Noorwez, S. M., Kaushal, S., Kono, M., and Moritz, O. L. (2014) Photoactivation-Induced Instability of Rhodopsin Mutants T4K and T17M in Rod Outer Segments Underlies Retinal Degeneration in X. laevis Transgenic Models of Retinitis Pigmentosa. *J Neurosci* **34**, 13336-13348
61. Orisme, W., Li, J., Goldmann, T., Bolch, S., Wolfrum, U., and Smith, W. C. (2010) Light-dependent translocation of arrestin in rod photoreceptors is signaled through a phospholipase C cascade and requires ATP. *Cellular signalling* **22**, 447-456
62. Majumder, A., Pahlberg, J., Boyd, K. K., Kerov, V., Kolandaivelu, S., Ramamurthy, V., Sampath, A. P., and Artemyev, N. O. (2013) Transducin translocation contributes to rod survival and enhances synaptic transmission from rods to rod bipolar cells. *Proc Natl Acad Sci U S A* **110**, 12468-12473

Acknowledgements--Authors thank Darwin Toledo and other Garriga laboratory members for helpful discussion during the preparation of this manuscript. This work has been supported by grant SAF2011-30216-C02-01 from MICINN and Grups de Recerca Consolidats de la Generalitat de Catalunya (2009 SGR 1402) to PG, and the RP Fighting Blindness and Wellcome Trust to MEC. ER and AC are the recipients of Beatriu de Pinós Fellowships from AGAUR and a contract grant from the Instituto de Salud Carlos III, respectively. SS and XD are the recipients of pre-doctoral scholarship FI from AGAUR and Chinese Scholarship Council, respectively. ATM and ARW are supported by the National Institute for Health Research Biomedical Research Centre at Moorfields Eye Hospital NHS Foundation Trust and UCL Institute of Ophthalmology.

Footnotes

The abbreviations used are: DM, n-Dodecyl-D-Maltoside; ER, endoplasmic reticulum; FAF, fundus autofluorescence imaging; GPCR, G-protein-coupled receptor; Gt, transducin; MetaII, metarhodopsinII; OCT, Optical Coherence Tomography; PEI, polyethylenimine; PM, plasma membrane; Rh, rhodopsin; RP, retinitis pigmentosa; SB, Schiff base; TM, transmembrane.

FIGURE LEGENDS

Figure 1. ***Representative fundus images from patients with RHO p.N55K.*** Color fundus images of patient GC18466 showing no progression from years 41 (A) to 45 (B). (C-H) Autofluorescence images right (C, E, G) and left eyes (D, F, H) of GC18466 13 years (C, D), GC16563 39 years (E, F) and GC18466 45 years (G, H). OCT images of GC18466 13 years left eye (I) and GC18466 45 years right eye (J).

Figure 2. ***Representative images from patient with RHO p.M39R.*** Autofluorescence images, 55 degrees of field of six patients, each heterozygous for *RHO*, p.M39R presented in ascending age. (A) GC97/son, 28 years, (B) GC19172 29 years, (C) GC414 48 years; (D) GC109 50 years, (E) GC97/father 57 years, (F) GC4740 68 years. Hyperfluorescent rings delineate normal retina in the two youngest individuals.

Figure 3. ***The environment of positions M39$^{1.34}$ and N55$^{1.50}$ in dark-state and active (rhod)opsin crystal structures.*** A, B) Lateral (A) and extracellular (B) views of the proposed entry/exit channel for retinal between TMs 1 and 7, in the vicinity of M39$^{1.34}$. C) The polar cluster at the cytoplasmic side of TMs 1, 2 and 7 close to N55$^{1.50}$. Helices are displayed as *cartoon*, the relevant side-chains are shown as *sticks* colored by atom type and crystallographic water molecules as *spheres*. Dark-state crystal structures (PDB ids 1GZM, 1L9H and 1U19) are shown in *orange* and active-like structures (3DBQ, 2X72 and 3PQR) are in *red*. The side-chains of M/R39 (A, B) and N/K55 (C) are shown with a transparent *surface*. (hydroxyethyloxy)tri(ethyloxy)octane, palmitoyl and octyl glucoside (in A) and retinal molecules (in B) are shown with *ball-and-sticks*. The image was created using PyMol (Schrodinger, LLC. The PyMOL Molecular Graphics System, Version 1.5).

Figure 4. ***Subcellular localization of WT, and M39R and N55K mutants in SK-N-SH cells.*** (A and B) Representative images of rod opsin WT, M39R, N55K localization. SK-N-SH cells were transfected with WT and mutant rod opsins and 24 h later, cells were fixed. (A) Rh-1D4 primary antibody (green) was used to compare localization with BiP (red) following cell permeabilization with Triton X100. (B) The Rh antibody to an extracellular epitope 4D2 was used on non-permeabilized cells to show traffic to the cell surface. Images were taken using a Carl Zeiss LSM 710 laser-scanning confocal

microscope. Scale bar=10μm. (C) Quantification of opsin localization. Cells were scored for the predominant opsin localization at the PM (open bars) or overlap with an ER marker (grey bars) in approximately 400 cells. Error bars represent ± 2SE. (D) Western blot of WT, N55K and M39R transfected SK-N-SH cell lysates for rod opsin expression detected with Rh-1D4. 10 μg of soluble cell lysate protein (S) was compared to 10 μg of lysate digested with EndoH (E), or PNGase F (P). The asterisk (*) highlights the position of deglycosylated rod opsin and (**) the position of opsin dimer. ER retained opsin is sensitive to EndoH, whereas all opsin is sensitive to PNGase F and will tend to dimerize. The position of molecular weight markers is indicated on the left in kDa.

Figure 5. ***UV-vis characterization for the immunopurified WT and RP mutant pigment.*** UV-vis spectra of WT (A), M39R (B) and N55K (C), in the basal state (—) and upon light stimulation (---) are shown. Spectra were recorded in buffer C at 20ºC. N55K mutant presents lower chromophoric band compared to WT, with a slightly blue-shifted maximum (3 nm) according to UV-*vis* spectrophotometric measurements. Insets show the visible region for both dark and illuminated samples.

Figure 6. ***Chemical and thermal stability for WT, and RP mutants.*** WT, M39R, and N55K in buffer C were treated with 50 mM hydroxylamine pH 7.0 at 20ºC for the chemical stability assay. Thermal stability assay was carried out at 48ºC. (A) Chemical reagent stability was determined by monitoring the decrease of λmax over time (at 498nm for WT and M39R, and at 495nm for N55K) (B) Thermal stability assay plot showing the decrease of absorbance at the at the λmax in the visible region over time.

Figure 7. ***MetaII decay for WT and RP mutants.*** WT, M39R, and N55K in buffer C were illuminated and the Trp fluorescence increase at 330 nm was monitored in order to follow ligand release (38). After fluorescence stabilization, 50 mM Hydroxylamine pH 7.0 was added to confirm complete retinal release. Fluorescence intensity spectra of MetaII decay for WT, M39R and N55K are shown.

Figure 8. ***Gt activation by WT and RP mutant opsin and Rh.*** WT and RP mutants opsin (open circles) and Rh (closed circles) activity were measured by means of a radionucleotide filter-binding assay in COS-1 cell membranes in buffer Gt. The mean and standard error of three independent measurements are represented.

Rh	**WT**	**M39R**	**N55K**
A_{max} (dark) (nm)	498	498	495
[a]Ratio	2.5 ± 0.1	6.0 ± 2.0	5.4 ± 0.3
[b]Thermal Stability (48ºC) (min)	26.5 ± 1.5	2.1 ± 0.3	2.1 ± 1.0
[c]Hydroxylamine 50 mM (20ºC) Initial Velocity (min^{-1})	0.00036 ± 0.00016 (1)	0.00135 ± 0.0005 (3.75)	0.0181 ± 0.0045 (50.2)
[d]MetaII Decay (20ºC) (min)	14.3 ±1.3	10.8 ± 0.5	14.7 ± 1.3
[e]Gt activation intial rate (min^{-1})	0.0875 ±0.0141 (1)	0.3± 0.03 (3.4)	0.0273 ± 0.0056 (0.3)

Table 1: ***Spectroscopic properties of WT and RP mutants Rh.*** [a]The ratio of A_{280} /A_{max}, provides a measurement of sample purity and ability of opsin to form pigment with the chromophore. [b]Thermal bleaching $t_{½}$ values of purified samples in buffer C at 48ºC derived from the time course decay of the visible absorbance band at λ_{max}. [c]Hydroxylamine reactivity of the dark state pigments at 20ºC. Values were determined by monitoring the rate of λ_{max} absorbance decrease after the addition of 50 mM hydroxylamine (pH 7.0) to the samples in buffer C and adjusted to a single exponential decay function for the N55K RP mutant or a linear function for WT and M39R. For a better comparison of initial velocity values, relative data are shown in parenthesis. [d]MetaII stability $t_{1/2}$ values were determined by fitting the experimental data to a single-exponential curve of Trp fluorescence increase, due to the retinal release at 20ºC (38). [e]Gt activation initial rate was calculated as previously described (45). In all cases, mean values and standard error were obtained from three independent experiments.

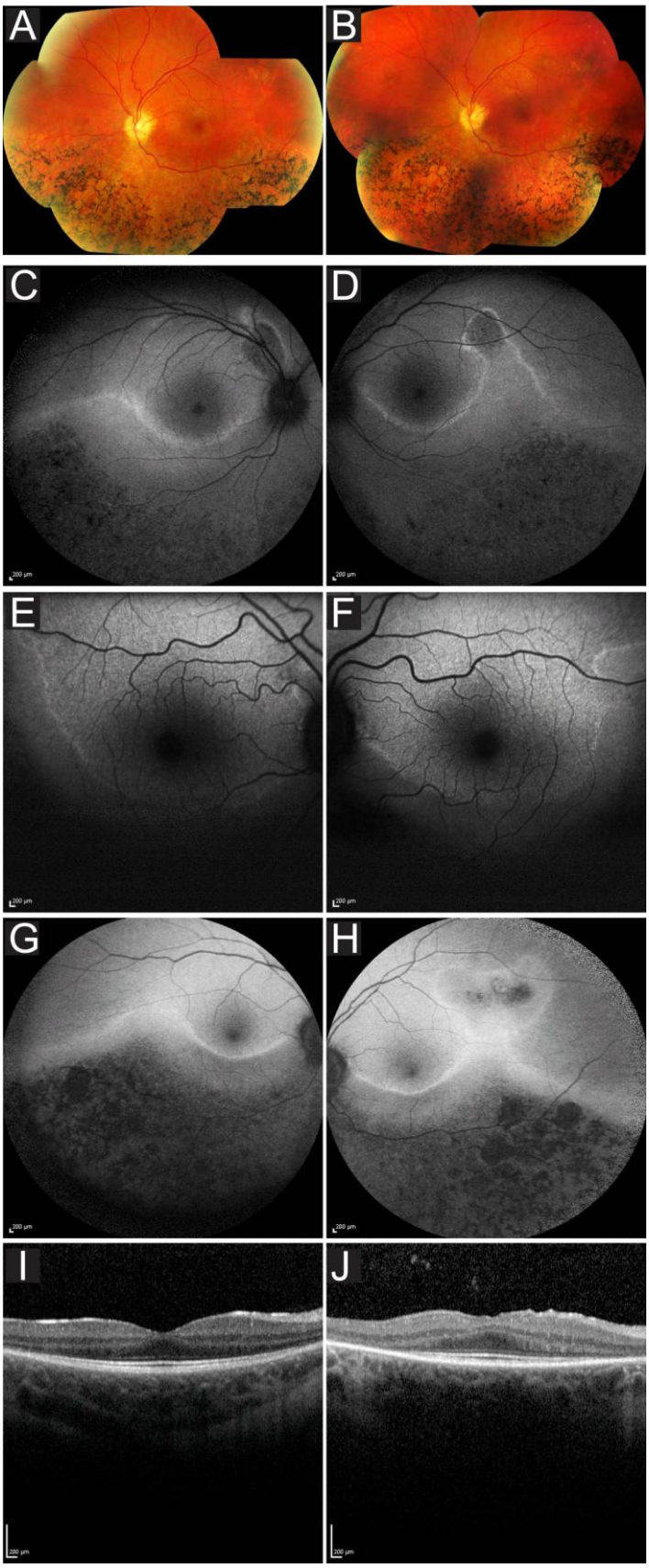

Figure 1

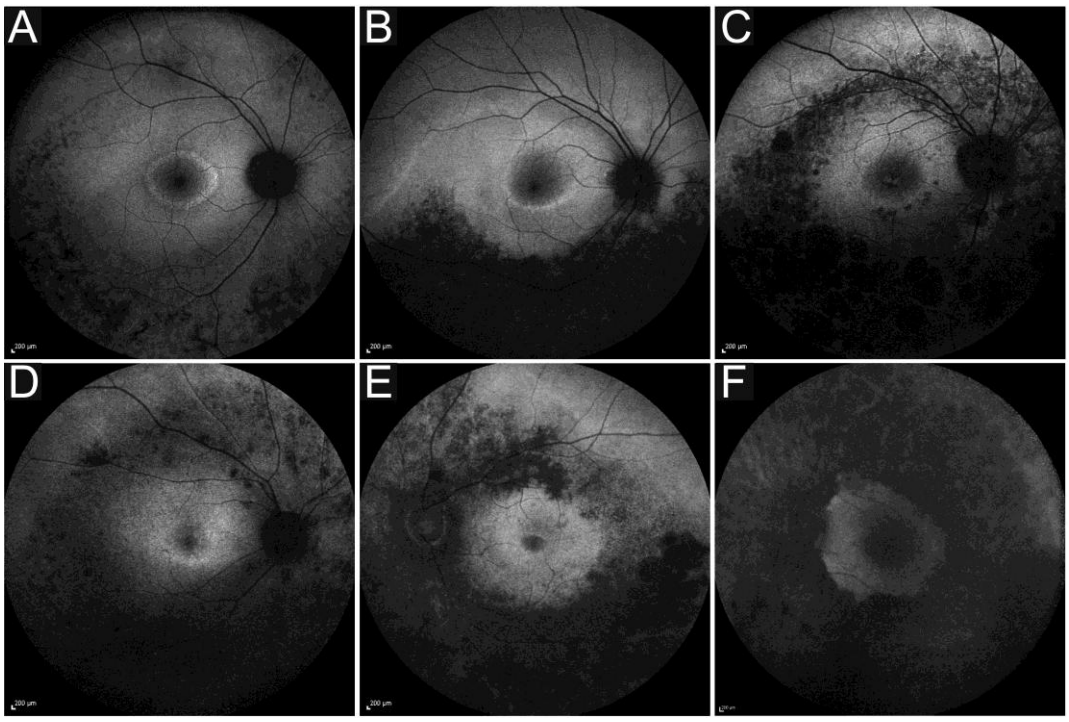

Figure 2

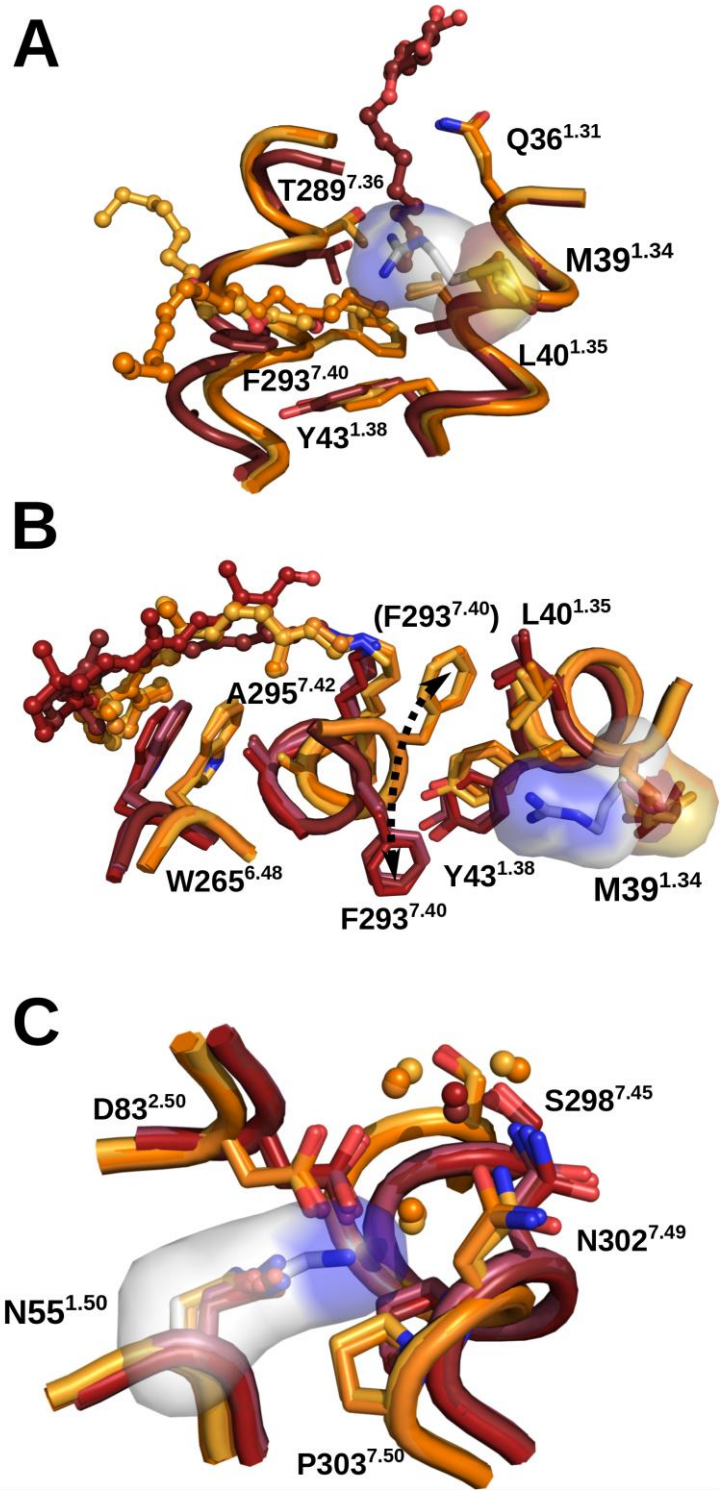
A
Q36^1.31
T289^7.36
M39^1.34
L40^1.35
F293^7.40
Y43^1.38
B
(F293^7.40)
L40^1.35
A295^7.42
W265^6.48
Y43^1.38
M39^1.34
F293^7.40
C
D83^2.50
S298^7.45
N302^7.49
N55^1.50
P303^7.50

Figure 3

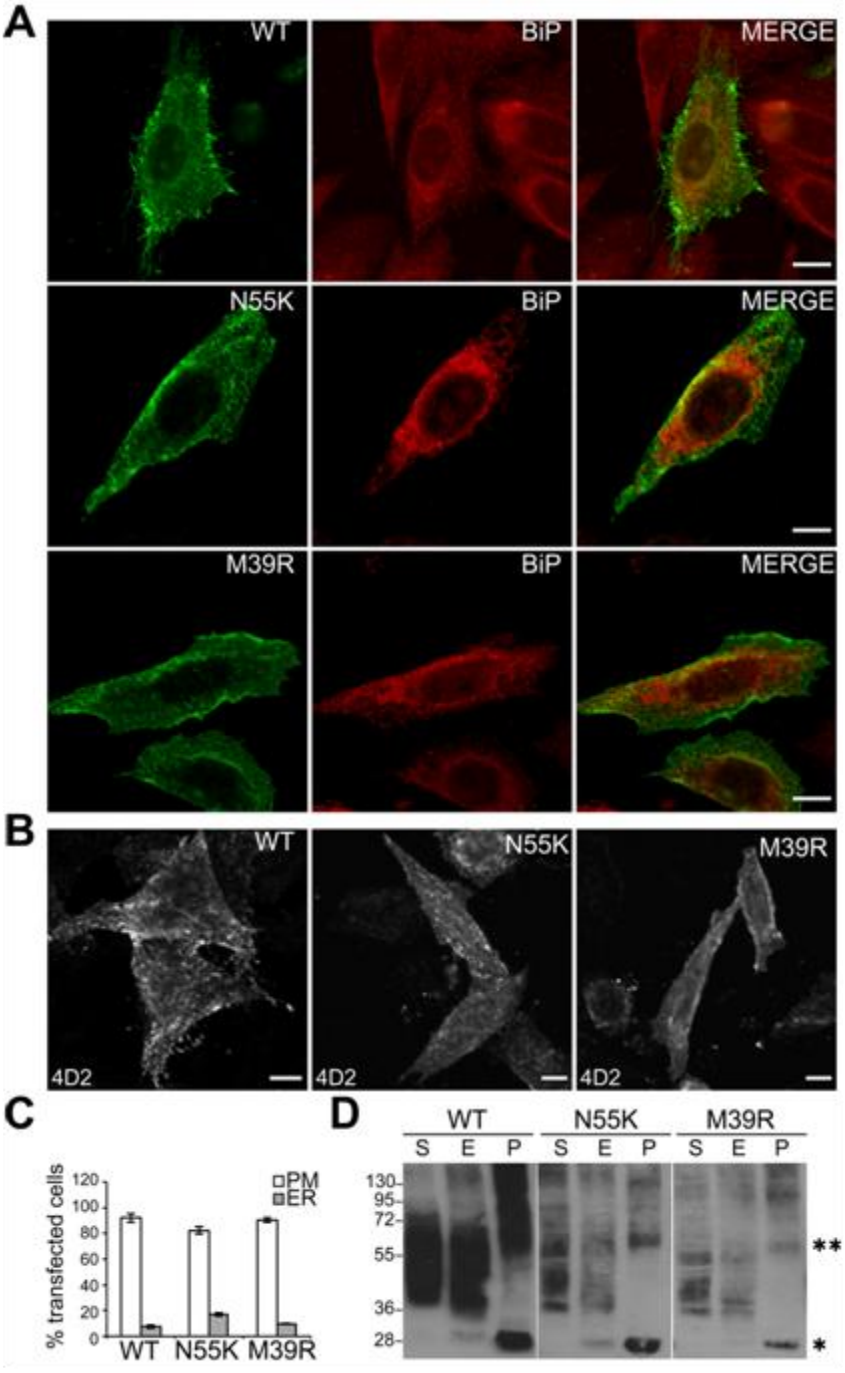
A
WT
BiP
MERGE
N55K
BiP
MERGE
M39R
BiP
MERGE
B
WT
N55K
M39R
4D2
4D2
4D2
C
% transfected cells
120
100
80
60
40
20
0
PM
ER
WT
N55K
M39R
D
WT
N55K
M39R
S
E
P
S
E
P
S
E
P
130
95
72
55
36
28
**
*

Figure 4

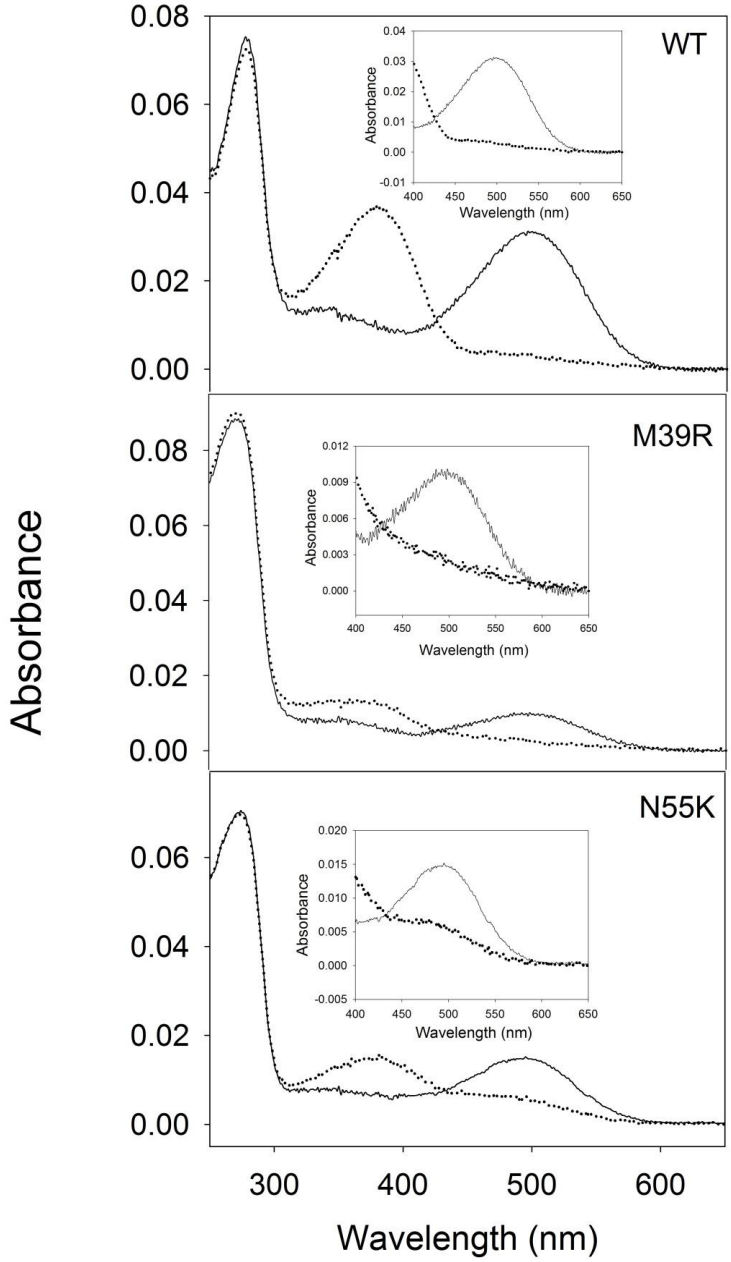
WT
M39R
N55K
Absorbance
Wavelength (nm)
0.08
0.06
0.04
0.02
0.00
300
400
500
600
0.04
0.03
0.02
0.01
0.00
-0.01
0.012
0.009
0.006
0.003
0.000
0.020
0.015
0.010
0.005
0.000
-0.005
400
450
500
550
600
650

Figure 5

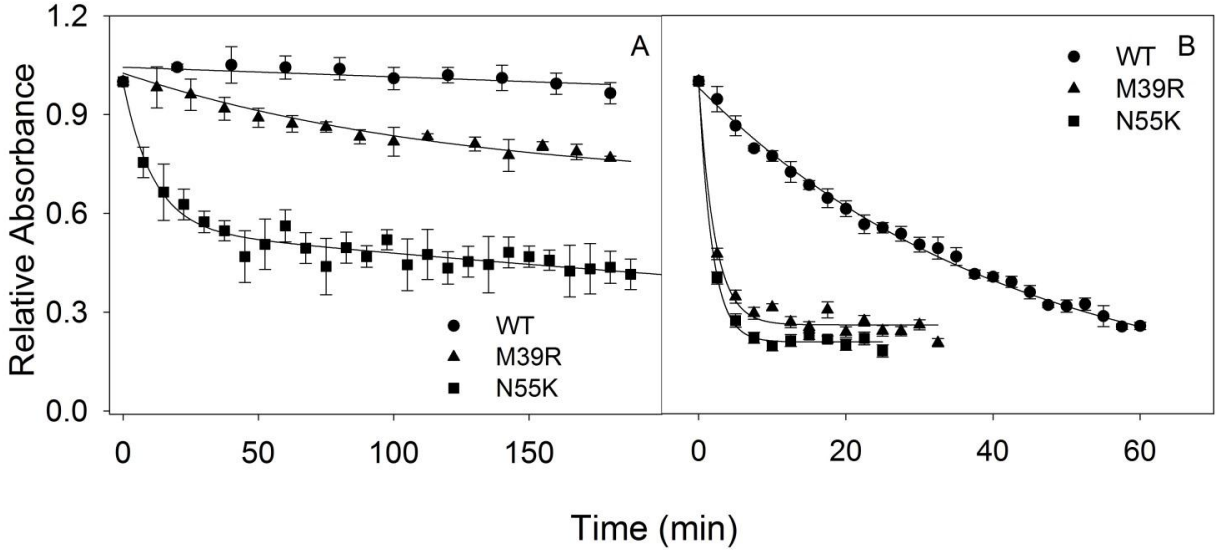
Relative Absorbance
1.2
0.9
0.6
0.3
0.0
A
B
WT
M39R
N55K
0
50
100
150
0
20
40
60
Time (min)

Figure 6

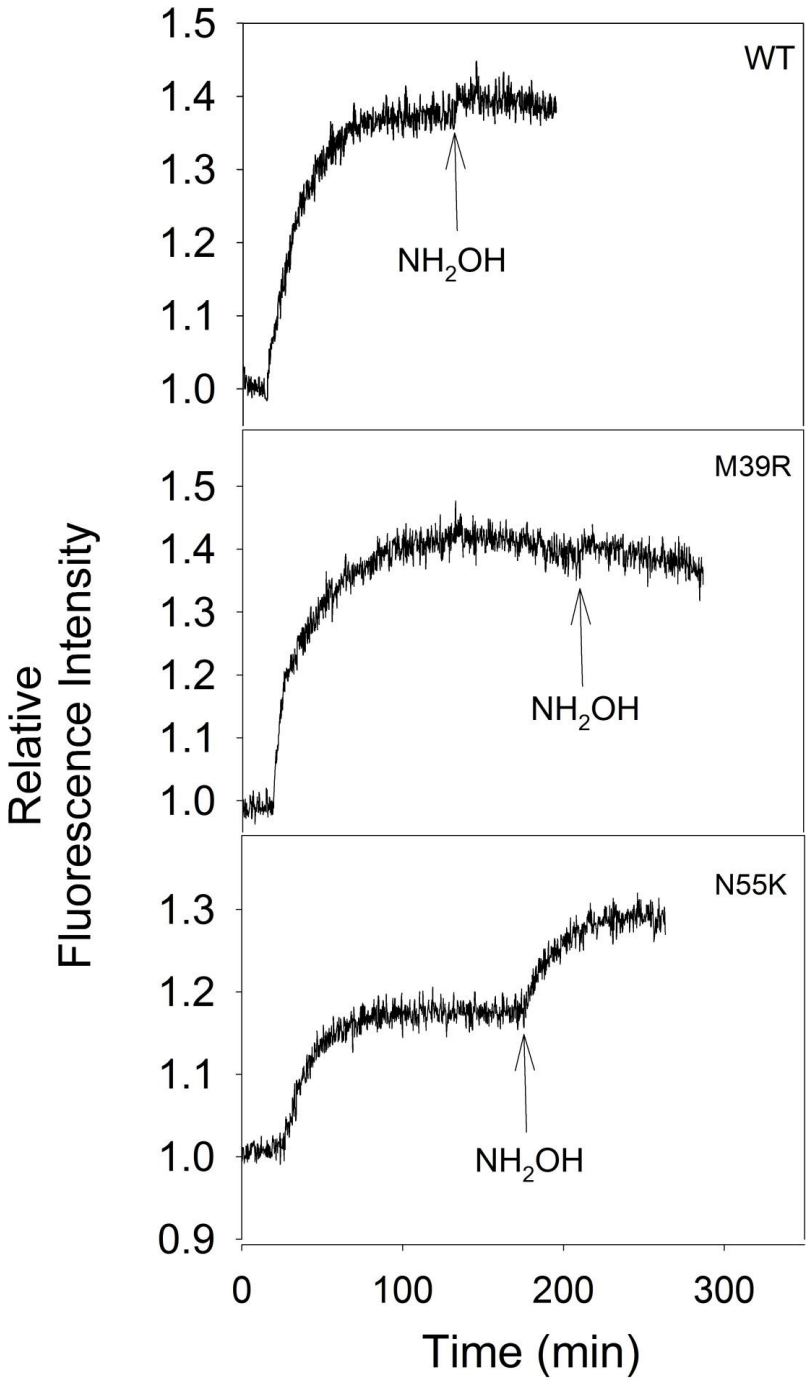
Relative Fluorescence Intensity
WT
M39R
N55K
NH2OH
NH2OH
NH2OH
1.5
1.4
1.3
1.2
1.1
1.0
0.9
0
100
200
300
Time (min)

Figure 7

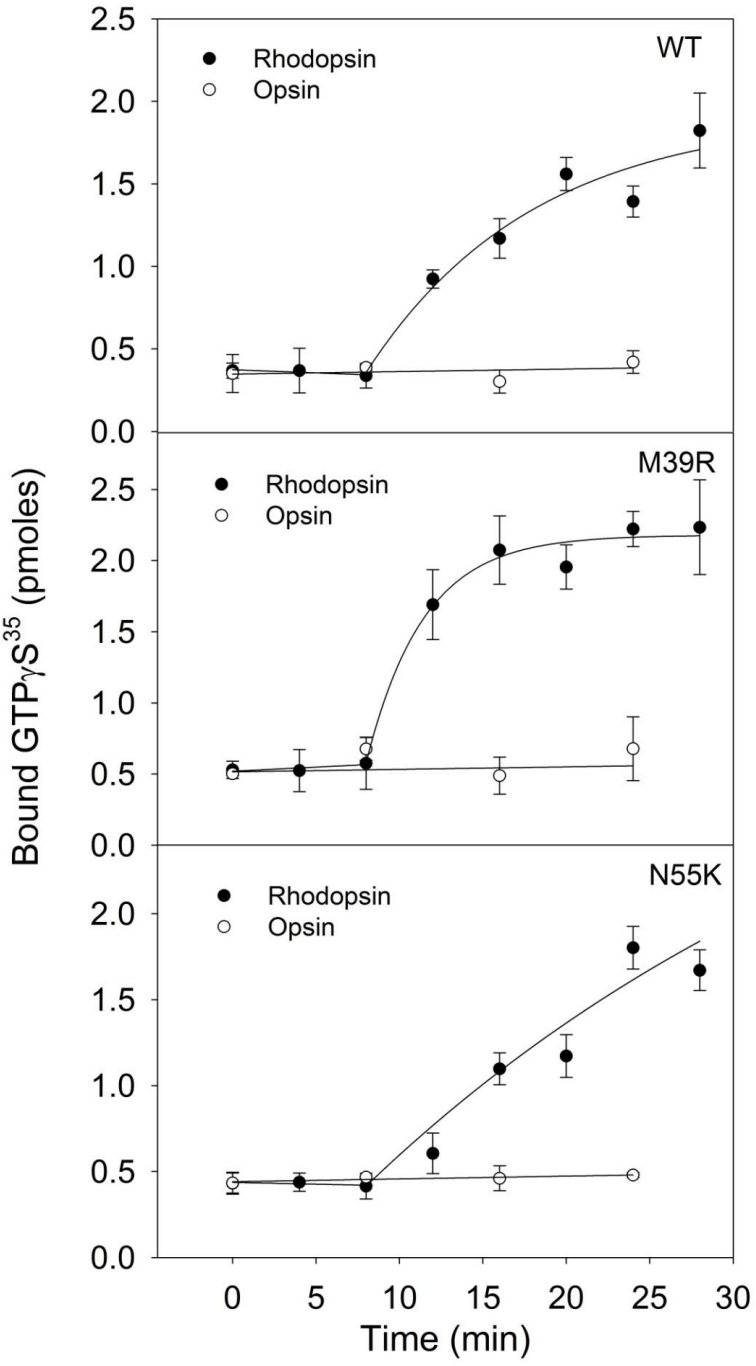
WT
Rhodopsin
Opsin
M39R
Rhodopsin
Opsin
N55K
Rhodopsin
Opsin
Bound GTPγS35 (pmoles)
Time (min)
0.0
0.5
1.0
1.5
2.0
2.5
0
5
10
15
20
25
30

Figure 8